AD A107664

MARTIN MARIETTA

Martin Marietta
Laboratories

LEVEL

MML TR 81-45c

EFFECTS OF SURFACE MORPHOLOGY AND CHEMICAL COMPOSITION ON THE DURABILITY OF ADHESIVELY BONDED ALUMINUM STRUCTURES

October 1981

Final Report

DTIC

NOV 2 0 1981

H

Prepared by:

T.S. Sun
G.D. Davis
J.D. Venables
J.M. Chen

Martin Marietta Corporation
Martin Marietta Laboratories
1450 South Rolling Road
Baltimore, Maryland 21227

81   56

REPORT DOCUMENTATION PAGE		READ INSTRUCTIONS BEFORE COMPLETING FORM
1. REPORT NUMBER AFOSR-TR- 81-0725	2. GOVT ACCESSION NO.	3. RECIPIENT'S CATALOG NUMBER
4. TITLE (and Subtitle) Effects of Surface Morphology and Chemical Composition on the Durability of Adhesively Bonded Aluminum Structures		5. TYPE OF REPORT & PERIOD COVERED Final Report
		6. PERFORMING ORG. REPORT NUMBER
7. AUTHOR(s) T.S. Sun, G.D. Davis, J.D. Venables, J.M. Chen		8. CONTRACT OR GRANT NUMBER(s) F 49620-78-C-0097
9. PERFORMING ORGANIZATION NAME AND ADDRESS Martin Marietta Corporation Martin Marietta Laboratories 1450 South Rolling Road, Baltimore, MD 21227		10. PROGRAM ELEMENT, PROJECT, TASK AREA & WORK UNIT NUMBERS 61102F 2305/A2
11. CONTROLLING OFFICE NAME AND ADDRESS Air Force Office of Scientific Research/NC Bolling Air Force Base, Washington, D.C. 20332		12. REPORT DATE October 1981
		13. NUMBER OF PAGES 36
14. MONITORING AGENCY NAME & ADDRESS(If different from Controlling Office)		15. SECURITY CLASS. (of this report) Unclassified
		15a. DECLASSIFICATION DOWNGRADING SCHEDULE

16. DISTRIBUTION STATEMENT (of this Report)

Approved for public release, distribution unlimited.

17. DISTRIBUTION STATEMENT (of the abstract entered in Block 20, if different from Report)

18. SUPPLEMENTARY NOTES

19. KEY WORDS (Continue on reverse side if necessary and identify by block number)

anodic coatings - aluminum, phosphoric acid anodization, oxide morphology, hydration, surface composition, scanning transmission electron spectroscopy, X-ray photoelectron spectroscopy, adhesive bonding, surface behavior diagrams

20. ABSTRACT (Continue on reverse side if necessary and identify by block number)

(over)

DD FORM 1473 1 JAN 73

Unclassified

SECURITY CLASSIFICATION OF THIS PAGE (When Data Entered)

The hydration of aluminum surfaces prepared for adhesive bonding by anodization in phosphoric acid has been studied using surface behavior diagrams. These surface behavior diagrams, which are similar to phase diagrams for equilibrium bulk phases, trace the evolution of the aluminum adherend surface composition, obtained by X-ray photoelectron spectroscopy, during the hydration process. When supplemented with high resolution scanning electron micrographs and Auger depth profiles, the surface behavior diagrams show that hydration proceeds in three steps. The first is reversible and consists of the adsorption of water by the monolayer of $AlPO_4$ initially present on the surface. It involves no change in the oxide morphology. The second, which appears to be rate controlling, involves the slow dissolution of the phosphate followed by rapid hydration of the exposed alumina to the oxyhydroxide, boehmite. During this stage, extensive morphological changes occur as the boehmite fills the pore cells and bridges the whiskers of the original surface. The final step consists of the nucleation and growth of the trihydroxide, bayerite, on top of the boehmite. Using these results as examples, we propose the surface behavior diagram approach as a new tool for the study of surface reactions in general.

MML TR 81-45c

EFFECTS OF SURFACE MORPHOLOGY AND CHEMICAL COMPOSITION ON THE

DURABILITY OF ADHESIVELY BONDED ALUMINUM STRUCTURES

Final Report

Prepared by:

T.S. Sun
G.D. Davis
J.D. Venables
J.M. Chen

Martin Marietta Corporation
Martin Marietta Laboratories
1450 South Rolling Road
Baltimore, Maryland 21227

Prepared for:

Department of the Air Force
Air Force Office of Scientific Research
Bolling Air Force Base
Washington, D.C.   20332

Principal Investigators:

T.S. Sun

G.D. Davis

J.D. Venables

J.M. Chen

AIR ____ _____ _____ (AFSC)
_____
_____
_____ and is
_____ 190-12.
_____
Chief, _____ Information Division

FOREWORD

This document is the final report on work done by Martin Marietta Laboratories (MML) under the Air Force Office of Scientific Research Contract F49620-78-C-0097. This report completes the Laboratories' required work under the contract.

The principal investigators at the Labs were Drs. Guy D. Davis and Tsishung Sun. Co-principal investigators were Drs. John D. Venables and Jar-Mo Chen. Mr. Robert C. Butler performed the hydration and X-ray photoemission measurements.

TABLE OF CONTENTS

LIST OF FIGURES

LIST OF TABLES

I. INTRODUCTION

During the last four years, investigators at Martin Marietta Laboratories have conducted a comprehensive investigation to determine the fac s responsible for promoting the integrity and long-term durability of adhesively bonded aluminum structures. Two extremely important concepts have evolved from this work. First, it has been clearly demonstrated that the microscopic roughness of the oxide surface on Al is the single most critical factor in determining initial bond strength.[1] Rough and porous oxides are produced by various etching and anodizing pretreatment processes, such as the Forest Products Laboratory (FPL) sulfuric acid-sodium dichromate etch,[2] phosphoric acid anodization (PAA),[3] and chromic acid anodization (CAA).[4] The rough surface is important because it mechanically interlocks with the overlying polymer to form a much stronger bond than is possible with a smooth oxide.

The second important finding is that the long-term durability of aluminum/polymer bonds is determined almost exclusively by the degree of stability of the aluminum oxide in a humid environment.[5] Moisture transforms the oxide to a hydroxide with an accompanying morphological change. The resulting material, the boehmite form of aluminum hydroxide, adheres poorly to the aluminum beneath it. Therefore, once it forms, the overall bond strength is severely degraded.

In the past year, we have made a dedicated effort to understand the oxide-to-hydroxide conversion process on aluminum. One of the techniques we have developed to study this problem is discussed here in

detail. In brief, we have used X-ray photoelectron spectroscopy (XPS) (also known as electron spectroscopy for chemical analysis [ESCA]) to provide data for generating surface behavior diagrams. This type of diagram, which is similar to a phase diagram for equilibrium bulk phases, is a convenient and potentially very powerful technique for tracing the evolution of surface reactions and the stability of adsorbed species. As far as we know, this is the first time that such an approach has been used in the study of surfaces and we suggest that it may find general applications in the surface science field.

The present study covers our investigations into the stability of aluminum surfaces that have been treated with the PAA process. Our objective was to determine why the PAA oxide is more stable in a humid environment than oxides produced by other adhesive bonding procedures.

II. EXPERIMENTAL TECHNIQUES

The XPS measurements were done with a Physical Electronics spectrometer (Model 548) featuring a double-pass cylindrical mirror analyzer (CMA) capable of Auger-electron spectroscopy (AES), X-ray photoelectron spectroscopy (XPS), and ultraviolet photoelectron spectroscopy (UPS). Several important features of this spectrometer were reported previously.(6-8) The X-ray source, which contains a Mg anode, has a characteristic Kα line at 1253.6 eV, and a line width of 0.6 eV without monochromatization. The energy resolution of the analyzer was set at ~ 4.0 eV for panoramic scans (with binding energies of 0 - 1000 eV) and at ~ 1.0 eV for individual peak analyses (with 10-20 eV ranges of binding energies). The high-resolution spectra were used to obtain line intensities and to determine peak positions.

The intensity of an XPS line was calculated from the area under the peak after a linear background subtraction. To perform quantitative analysis, the sensitivity factors of the major XPS lines, Al 2p, P 2p, and O 1s, were determined from the spectra of high-purity powders of α-Al_2O_3, γ-Al_2O_3, $AlPO_4$, and Na_3PO_4. As indicated in Table I, the sensitivity factors (normalized with respect to oxygen) agree fairly well with published values.(9) The relative elemental concentrations of a surface were determined from the intensities of the XPS lines of the various elements divided by the appropriate sensitivity factors and then normalized so that the total concentration of the individual elements added to 100%.

- 8 -

TABLE I

XPS Sensitivity Factors

Element	XPS Line	This Work	Ref. 9
O	1s	1.0	1.0
Al	2p	0.20	0.17
P	2p	0.51	0.40

The binding energy scale of the spectrometer was calibrated with reference to the Au $4f_{7/2}$ and C 1s peaks at 83.8 and 285.0 eV, respectively. However, since charging of non-conducting surfaces may shift observed binding energies uniformly, only differences in binding energies are reported.

Oxide morphology and hydrate structure were studied with a JEOL 100CX scanning transmission electron microscope (STEM), operated in the high resolution scanning mode. The details of STEM specimen preparation were described in a previous study.[1] To improve the topographic perception of the surface structures, we made stereo pairs (10° tilt angle) of all the micrographs at 50,000X, unless otherwise indicated.

The specimen strips (1 cm x 8 cm) were made from sheets of commercial 2024-T3 Al alloy with a nominal composition of 93.5% Al, 4.4% Cu, 1.5% Mg, and 0.6% Mn (by weight). They were pretreated with the Forest Products Laboratory (FPL) process,[2] which consists of degreasing, alkaline cleaning, and etching in a solution containing $Na_2Cr_2O_7 \cdot 2H_2O$, H_2SO_4, and H_2O in a 1:10:30 ratio by weight. After a thorough rinse, the specimens were anodized for 20 min in an aqueous solution of 10 wt.% H_3PO_4 at +10 V with respect to a Pt counter-electrode. The anodized specimens were rinsed with distilled water or, in some cases, with acetone, dried with warm air, and stored in a vacuum desiccator at room temperature.

The anodization produced an oxide film consisting of a thin (100 Å) barrier layer adjacent to the metal and a thick (~ 4000 Å) porous layer at the top. Researchers at the Labs have investigated several important characteristics of the oxide film.[1,5,6,10,11] The porous

layer consists of a thin barrier layer underneath closely packed pore cells, with fine whiskers at the top. Figure 1 shows stereo electron micrographs and an isometric drawing of the oxide morphology from a fresh specimen. The anodic oxide is composed predominantly of amorphous Al_2O_3. The major components of the alloy, Cu, Mg, and Mn, are not present in the oxide within the limit of the XPS detectivity ($\sim 0.1\%$).

Identically prepared PAA-Al coupons were exposed to air (at either 50° or 60°C) saturated with water vapor (100% relative humidity) in a Blue M temperature-controlled humidity chamber. The samples were suspended vertically so that condensation could drip off. The specimens were removed from the humid environment at different intervals, dried with forced air at room temperature, and stored in a desiccator prior to measurement with the STEM or the XPS spectrometer.

(a)

0.5μm

(b)
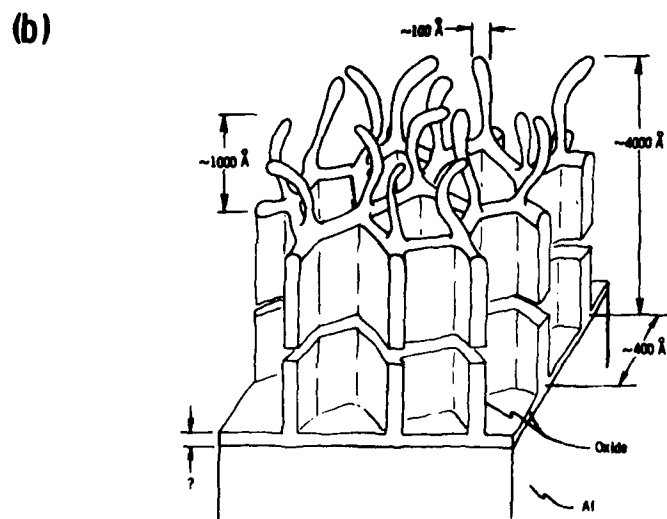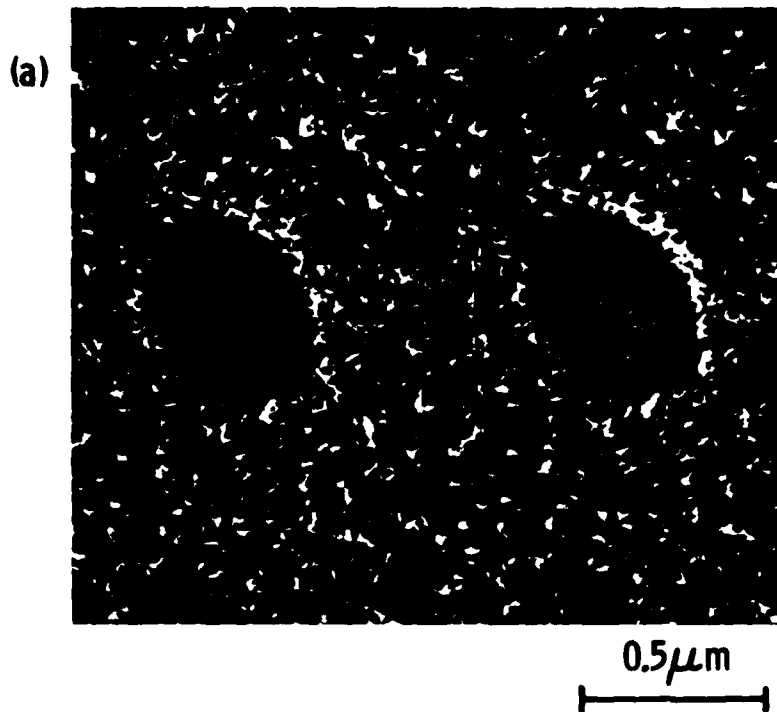
Figure 1. a) Ultra-high resolution stereo SEM micrograph and b) iso-
metric drawing of the oxide morphology on a PAA-treated
aluminum surface. The origin of the depressed region in the
oxide seen in a) is unknown, but may have been due to a gas
bubble that inhibited oxide growth. (50,000x)

- 12 -

III. RESULTS

A. Chemical Information from XPS

A typical XPS spectrum of the PAA oxide is shown in Fig. 2. Only four elements -- Al, P, C, and O -- are present on the surface. This result is consistent with that of a previous study based on Auger electron spectroscopy.[10] According to the Auger depth profiles, the hydrocarbon species is present only on the surface layer and is attributed to contamination. Based on the binding energy differences of their XPS lines, the chemical states of Al and P are identified as those of Al_2O_3 and a phosphate, presumably $AlPO_4$, respectively (Table II). Any excess oxygen, indicated by quantitative analysis, is assumed to be bonded to hydrogen, which cannot be detected directly by XPS, but which has been detected by infrared spectroscopy.[12,13] Since the hydration products of Al_2O_3 -- $AlOOH$ and $Al(OH)_3$ -- can be written in the form $Al_2O_3 \cdot nH_2O$, the surface composition can be represented as a linear combination of Al_2O_3, $AlPO_4$, and H_2O.

B. The Surface Behavior Diagram

The elementary composition defined from XPS measurements can be converted into a ternary composition $xAl_2O_3 + yAlPO_4 + zH_2O$. The measured intensity of the O 1s peak is assumed to be the total of the contributions from oxygen in Al_2O_3, $AlPO_4$, and H_2O. These two systems are related to each other through the following equations:
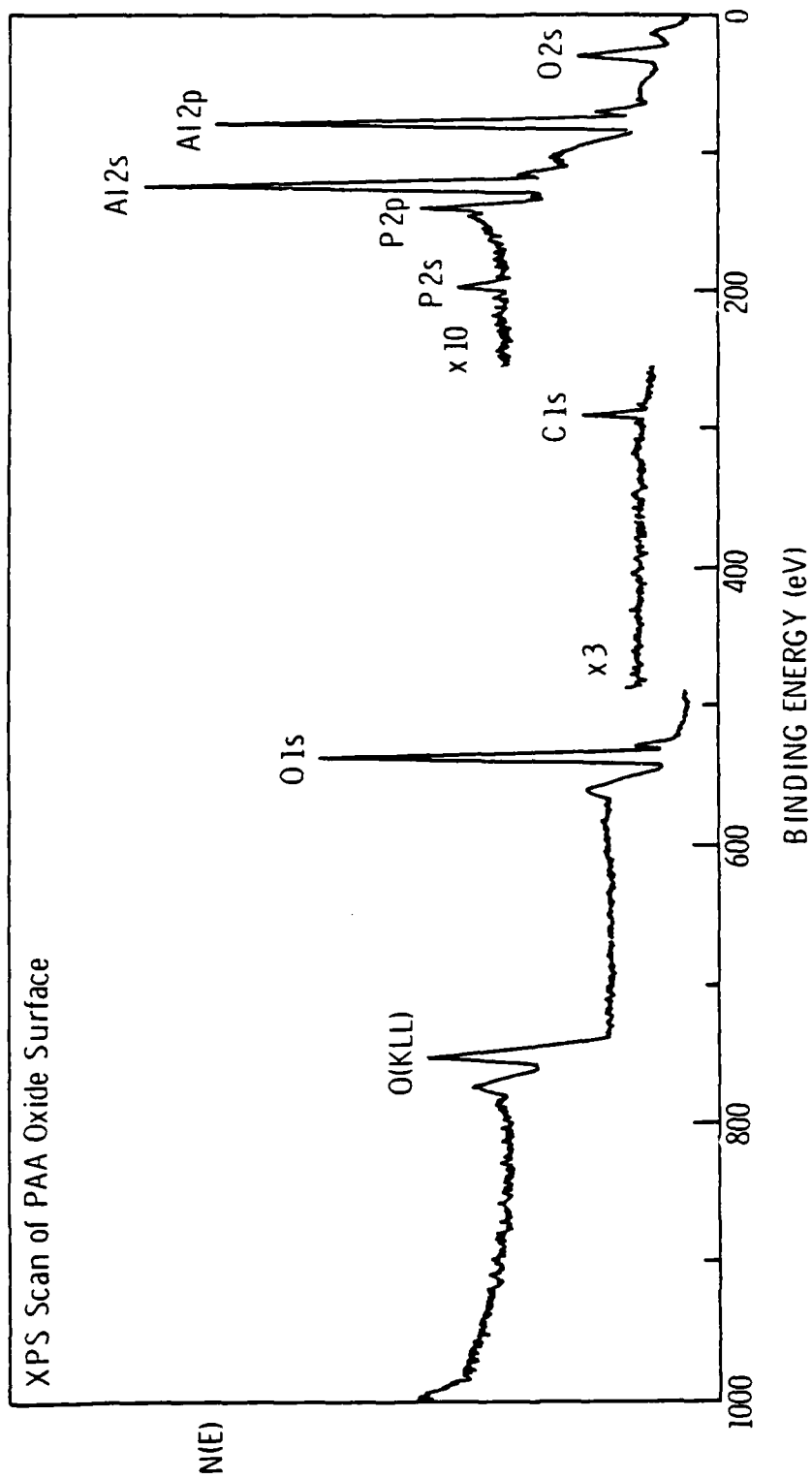
Figure 2. The X-ray photoelectron spectrum of a freshly prepared PAA-Al oxide surface.

Table II

Binding Energy Differences for Several Al- and P-Containing Compounds

Sample	Binding Energy Differences (eV)	
	(O 1s - Al 2p)	(O 1s - P 2p)
PAA surface	456.2 ± 0.4	396.7 ± 0.4
AlPO$_4$	456.4 ± 0.4	397.2 ± 0.4
Na$_3$PO$_4$		397.1 ± 0.4
Al$_2$O$_3$	456.0 ± 0.4	
Al(OH)$_3$	456.9 ± 0.4	

$$x = K(C_{A1} - C_P)$$

$$y = 2KC_P \tag{1}$$

$$z = K(2C_0 - 3C_{A1} - 5\,C_P) = 1 - x - y$$

where C is the relative atomic concentration of the element denoted by the subscript and $K = 1/2\,(C_0 - C_{A1} - 2C_P)^{-1}$, a normalization factor. Each composition can be plotted as a point (x, y, z) in the surface behavior diagram as shown in Fig. 3. The results for several known compounds and the PAA oxide specimens prepared under different conditions are shown in the behavior diagram and are discussed below.

Because the data obtained from Al_2O_3 and $AlPO_4$ were used as reference standards to determine the sensitivity factors of the elements, their experimental and calculated compositions are, by definition, identical. However, the agreement between the measured and calculated compositions of the two aluminum hydroxides, AlOOH and $Al(OH)_3$, validates the sensitivity factors used in this work.

C. The Initial Oxide Surface

The compositions of the PAA oxides lie along one of two tie lines: $AlPO_4-Al_2O_3$ or $AlPO_4 \cdot nH_2O-Al_2O_3$ (n < 1). The large variation in the $AlPO_4$ to Al_2O_3 ratios is attributed mainly to differences in the post-anodization rinse conditions. For example, coupons rinsed with acetone rather than water exhibited much higher phosphate concentrations and little, if any, detectable Al_2O_3. The $AlPO_4$ concentrations observed on water-rinsed surfaces range up to ~ 53% (Fig. 3, points a and a'), with the majority clustering at ~ 20%, a value corresponding to a monolayer
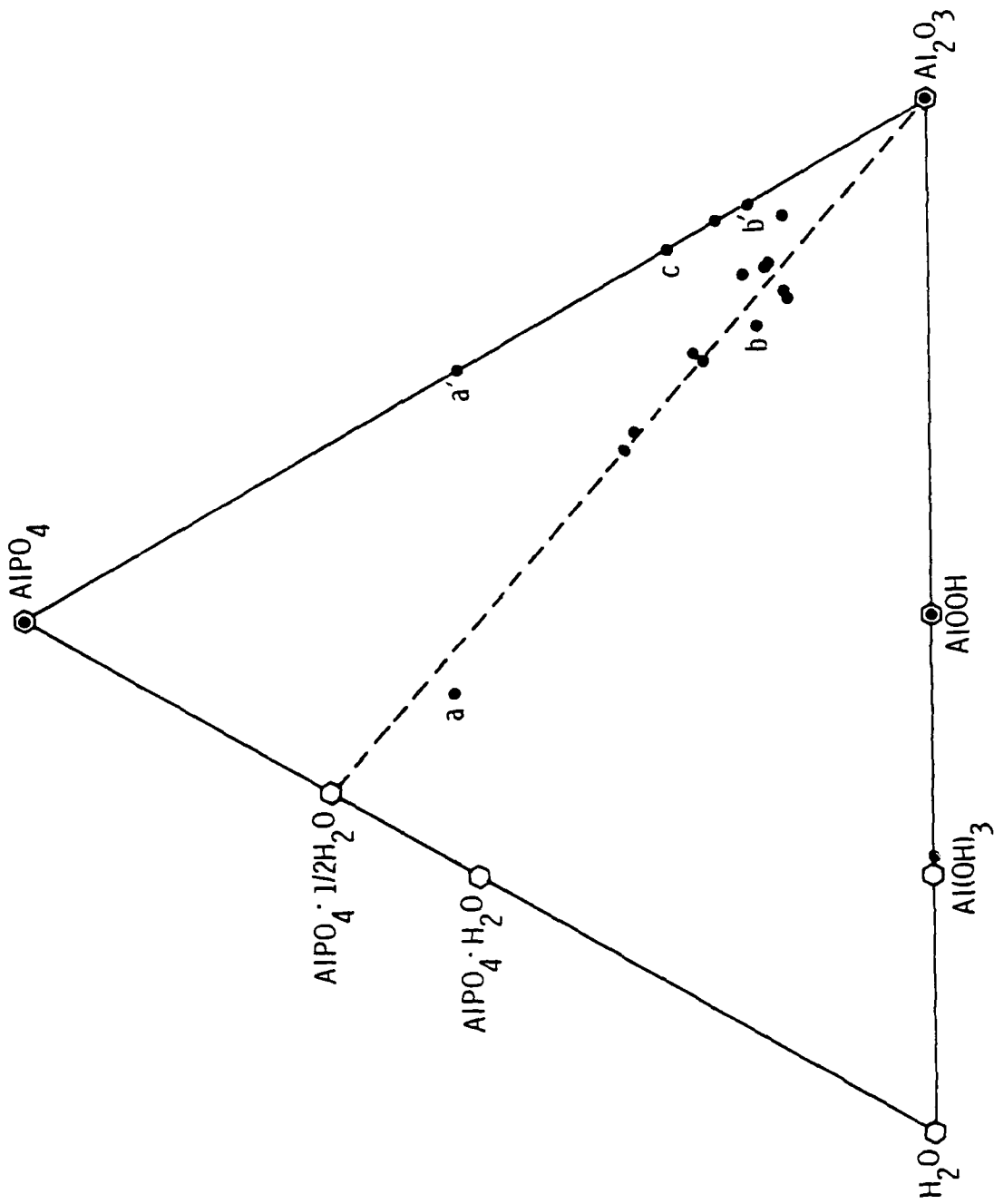
Figure 3. The $AlPO_4$ – Al_2O_3 – H_2O surface behavior diagram of the fresh PAA-Al oxide surface as determined by XPS measurements. The solid points are experimental compositions. The open points are calculated compositions. All surfaces were rinsed in water after anodization. Points a and a' and b and b' represent the same coupon before and after dehydration in an ultrahigh vacuum (see text).

of $AlPO_4$ on top of the Al_2O_3 substrate (assuming the mean free path
of the P 2p and Al 2p photoelectrons is 16 Å[14] and the average
thickness of one $AlPO_4$ layer is ~ 4 Å).

The majority of the PAA specimens exhibit some degree of hydration,
i.e., $z \neq 0$, due to the presence of the $AlPO_4 \cdot nH_2O$ phase, (n < 1).
However, dehydration occurred readily in vacuum as illustrated by two
pairs of data points, a-a' and b-b' (Fig. 3). The unprimed entries
represent the surface compositions shortly after the coupons were placed
in the ultrahigh vacuum (UHV) chamber and the primed entries represent
the compositions for the same specimens after they were kept in the vacuum
for three days. The latter points indicate a nearly total reduction of
water content. Another specimen, c, kept in a vacuum desiccator for 50
days before transfer to the UHV chamber, also exhibited an unhydrated
state. The scatter in composition along the horizontal direction, then,
is attributed primarily to the storage conditions of the specimens. As
a general rule, the longer the specimens were stored in vacuo, the closer
the composition to the $AlPO_4$-Al_2O_3 tie line. Furthermore, the oxide
morphology (as observed in the STEM) within each group of identically
anodized specimens is not detectably different despite the variation in
water content. These results suggest that the initial hydration stage
is reversible, involving the adsorption of water by the $AlPO_4$ on the
surface.

D.   Evolution of Surface Composition During Hydration

The results for a series of specimens that were prepared identically but exposed to 100% relative humidity at 50°C for various lengths of time are shown in the behavior diagram of Fig. 4. The exposure time (in hours) is indicated by the number adjacent to each data point. For comparison, the corresponding stereo micrographs of four of these specimens are shown in Fig. 5.

With 1- and 2-hour exposures, the H_2O concentration on the specimen surface increased slightly, but the composition remained near the $AlPO_4 \cdot nH_2O-Al_2O_3$ ($n < 1$) tie line. No change of oxide morphology was seen for these samples, indicating that the hydration activity at this early stage was confined to the first few atomic layers and probably involved the adsorption of water by the $AlPO_4$, as mentioned earlier.

When the exposure was increased from 2 to 4 hours, the surface composition evolved away from the $AlPO_4 \cdot nH_2O-Al_2O_3$ ($n < 1$) tie line. New structures, presumably some hydration product, appeared to grow around the whiskers, forming bridges between them, and, in some cases, covering the pores (Fig. 5). This stage marks the beginning of a more drastic hydration activity.

As the humidity exposure is increased further, the H_2O content increases at the expense of both Al_2O_3 and $AlPO_4$. The composition changed steadily along a straight line until it reached AlOOH (boehmite) at 96-hour exposure. From this point on, further exposure caused the composition to change along the $Al_2O_3-H_2O$ tie line toward the most advanced hydration

Figure 4. The surface behavior diagram of fresh and hydrated PAA–Al oxide surfaces. The numbers by some of the points denote the exposure in hours to 100% relative humidity at 50°C (solid points) or at 60°C (crosses).
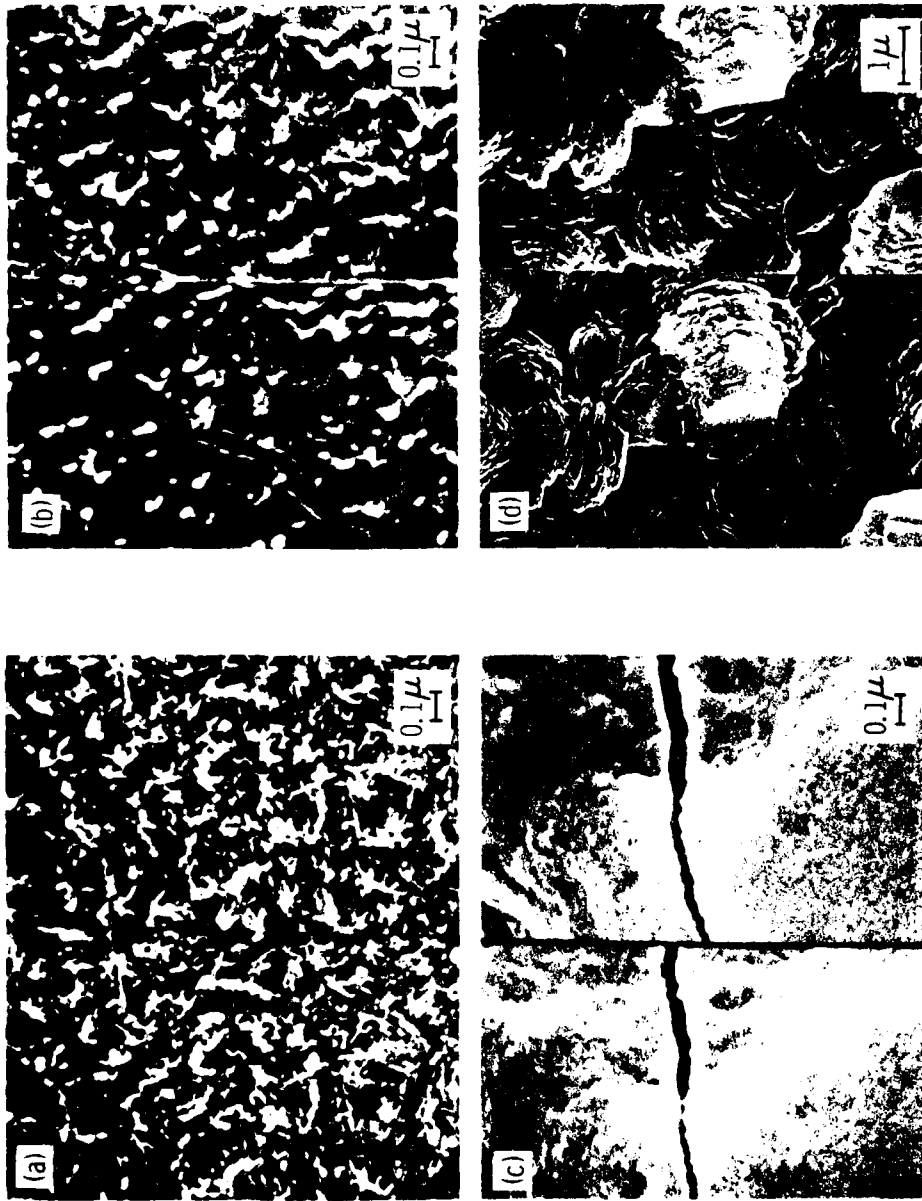
Figure 5. Stereo SEM micrographs of PAA Al oxide samples after exposure to 100% relative humidity at 50°C for a) 4 hours, b) 24 hours, c) 72 hours, and d) 192 hours.

- 21 -

state, i.e., Al(OH)$_3$ (bayerite), as indicated by the point for the specimen exposed 192 hours (Fig. 4).

The corresponding electron micrographs (Fig. 5) show that the hydration product nearly fills up the pores at 24-hour exposure and grows to an over-layer at 72 hr. Electron diffraction analyses made at both stages revealed the structure of a boehmite phase that corresponded to the composition data obtained with XPS. When the exposure is increased to 192 hours, crystallites of a second hydration product covered the specimen surface (Fig. 5d). An X-ray diffraction analysis on the layer covering this specimen revealed both bayerite and boehmite structures, with the first one dominant, i.e., a layer of bayerite has grown on top of the boehmite. These results are consistent with those of Vedder and Vermilyea(12,15) who used bulk-sensitive techniques and reported the formation of a pseudo-boehmite phase with a water content between that of boehmite and bayerite.

A second hydration experiment was performed at 60°C at 100% relative humidity. The hydration process again followed the same tie lines shown in the behavior diagram in Fig. 4. In general, less time was required for the hydration to occur at 60°C than 50°C, but there was considerable variation from sample to sample and across the same sample. We can correlate these variations with nonuniformities in phosphate coverage; the greater the phosphate concentration, the longer the time to hydration.(16)

IV. MODEL OF THE HYDRATION PROCESS

To help develop a model for the hydration process, we compared the expected surface composition changes with the experimental results for various possible reactions.

The initial specimen composition at a given stage is defined as $xAl_2O_3 + yAlPO_4 + zH_2O$, i.e., at the position (x,y,z) in the behavior diagram. At some small time interval later, the concentration changes to a new position $(x+\Delta x, y+\Delta y, z+\Delta z)$, where $\Delta x + \Delta y + \Delta z = 0$ (see Fig. 6). The direction of evolution is described by the angle α between the line connecting (x,y,z) and $(x+\Delta x, y+\Delta y, z+\Delta z)$ and the horizontal axis. It can be shown by trigonometric construction that:

$$\tan \alpha = \frac{\sqrt{3}}{1 + 2\Delta x/\Delta y}. \qquad (2)$$

This equation allows us to determine the direction of evolution with respect to the following possible reactions:

(a) _Hydration of surface $AlPO_4$ to form $AlPO_4 \cdot nH_2O$._ In this case, the $AlPO_4$ content does not change significantly, whereas the content of H_2O increases at the expense of detectable Al_2O_3, i.e., $\Delta z > 0$, $\Delta y \approx 0$, and $\Delta x \approx -\Delta z$. It follows that $\tan \alpha \simeq 0$ and $\alpha \simeq 0$. Thus, the surface composition evolves along the horizontal direction (path a in Fig. 7). The dehydration of $AlPO_4 \cdot nH_2O$ proceeds in the same way, but in the reverse direction.

This behavior can also be generalized to a surface containing no phosphate. The surface Al_2O_3 becomes hydrated and less of the underlying

- 23 -
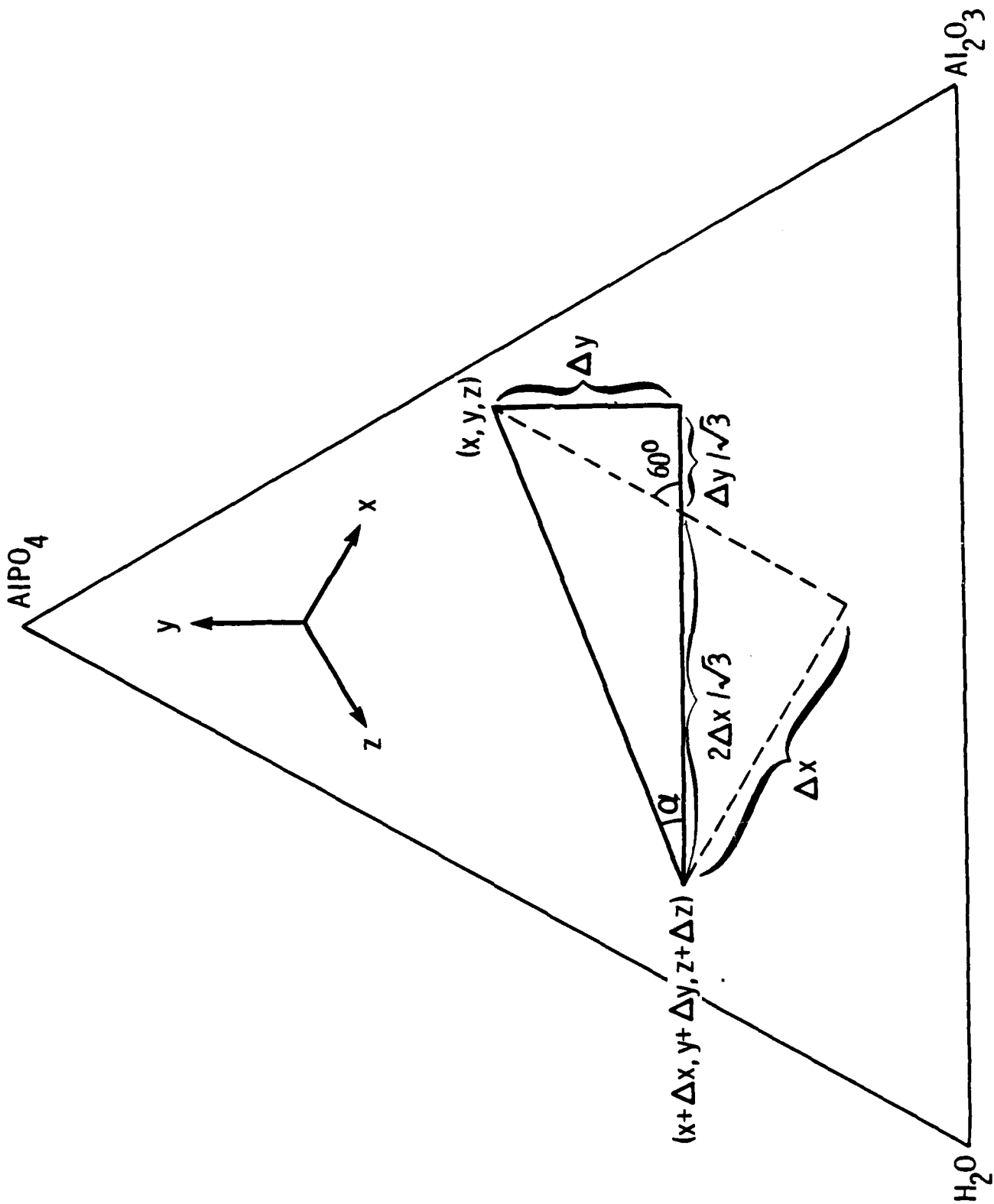
Figure 6. Surface behavior diagram illustrating the derivation of equation (2).
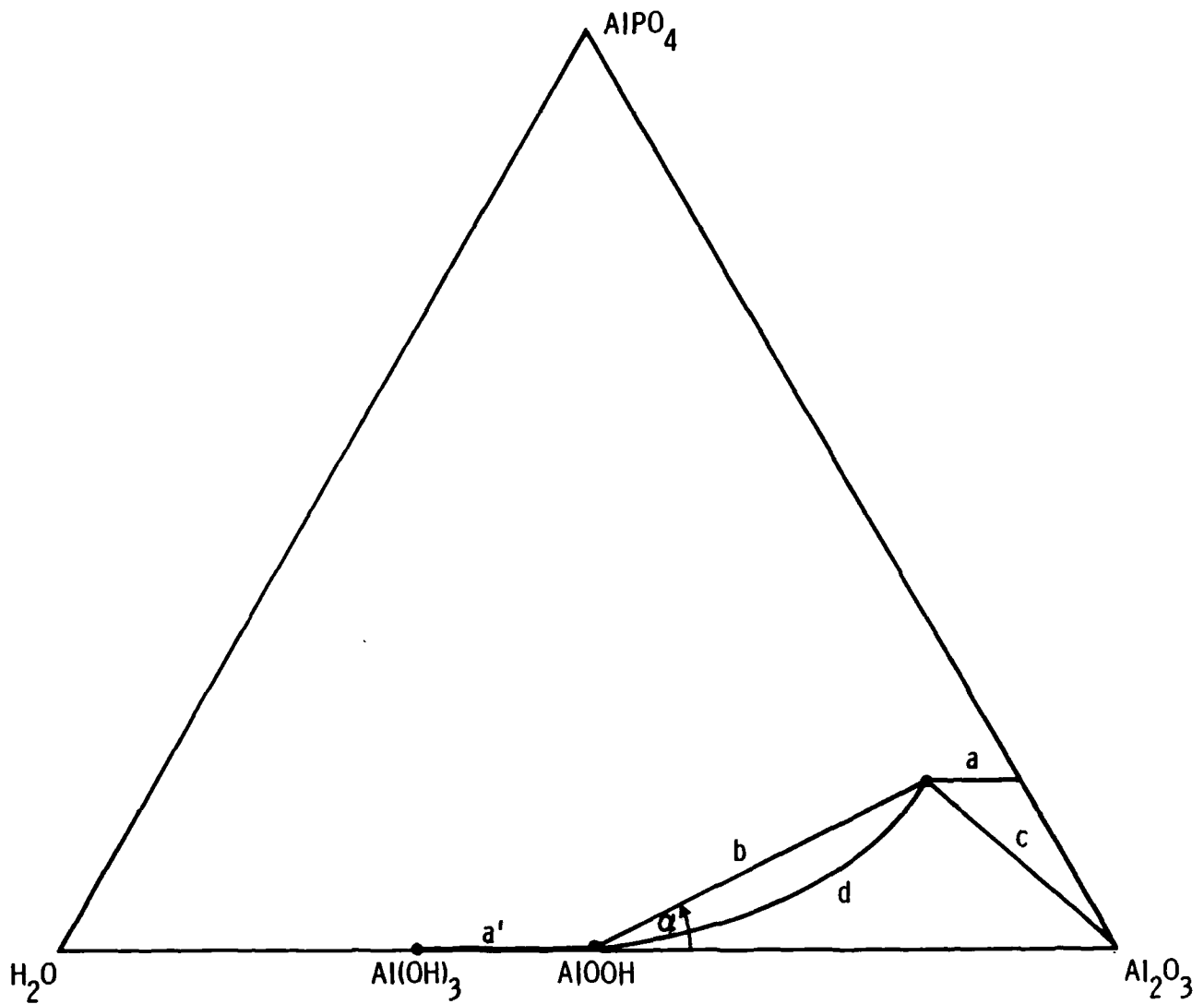
Figure 7. The surface behavior diagram showing different evolution paths
of surface composition: a) hydration of surface $AlPO_4$ to form
$AlPO_4 \cdot nH_2O$; a') hydration of surface $Al_2O_3 \cdot nH_2O$ to $Al_2O_3 \cdot mH_2O$,
$m > n$; b) nucleation and growth of a hydrated phase AlOOH;
c) dissolution of $AlPO_4 \cdot nH_2O$ without hydration of underlying
Al_2O_3; and d) dissolution of $AlPO \cdot mH_2O$ followed by hydration of
Al_2O_3.

Al_2O_3 is detected. The composition then follows the $Al_2O_3 - H_2O$ tie line (path a' in Fig. 7).

(b) <u>Nucleation and growth of a hydrated phase with composition</u> <u>$Al_2O_3 \cdot nH_2O$</u>. Phenomenologically, the surface coverage of $Al_2O_3 \cdot nH_2O$ increases with time at the expense of the original surface composition. The new surface composition can be expressed as

$$\delta Al_2O_3 \cdot nH_2O + (1-\delta') (xAl_2O_3 + yAlPO_4 + zH_2O)$$
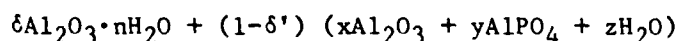
where δ denotes the increment of the hydrated phase and δ' the corresponding decrement of the original surface constituents. Thus $\Delta x = \delta - x\delta'$, $\Delta y = -y\delta'$, and $\Delta z = n\delta - z\delta'$. The requirement that $\Delta x = \Delta y + \Delta z = 0$ implies that $\delta' = (n+1)\delta$. Therefore, $\Delta x = [1-x(n+1)]\delta$, $\Delta y = -y(n+1)\delta$, and, accordingly,

$$\tan \alpha = \frac{\sqrt{3}}{1 + \frac{2}{y}\left[x - \frac{1}{n+1}\right]} \tag{3}$$

This tangent defines the tie line connecting the initial point (x,y,z) and the end point corresponding to $Al_2O_3 \cdot nH_2O$ on the behavior diagram (path b in Fig. 7). The composition of each point on the tie line is a linear combination of the two end points. When $n=1$, a special situation arises, and the end point corresponds to $AlOOH$.

(c) <u>Dissolution of $AlPO_4$ or $AlPO_4 \cdot nH_2O$ without hydration of the</u> <u>underlying Al_2O_3</u>. In this case, more Al_2O_3 is exposed, $\Delta x > 0$, and $AlPO_4$ and H_2O decrease proportionally $\Delta z = n\Delta y < 0$ and $\tan \alpha = - \frac{\sqrt{3}}{2n+1}$.

The surface composition evolves along a tie line connecting the initial point and that corresponding to Al_2O_3 (path c in Fig. 7).

(d)   Dissolution of $AlPO_4$ or $AlPO_4 \cdot nH_2O$ followed by hydration of the Al_2O_3. This case can be considered a combination of reactions (b) and (c). The initial and final compositions are the same as (b), but the phosphate concentration initially decreases more rapidly in this example. The composition of the surface evolves along a curve bounded by tie line b and tie lines c and $Al_2O_3-H_2O$ (path d in Fig. 7). The deviation of this curve from the straight line is a function of the relative kinetics of the two mechanisms. In the limiting case, i.e., where the dissolution of PO_4^{3-} proceeds slowly (i.e., it is the rate limiting step) and the hydration of the exposed surface follows quickly, the evolution of the surface oxide composition would be very similar to that of case b. These are, in fact, the expected relative rates of dissolution and hydration and to distinguish between the two cases, additional measurements are needed. The results of the measurements are discussed below.

Thus, the surface behavior diagram (Fig. 4) and the above analysis suggest a three-step model for the hydration process of the PAA oxide. In the first step, the surface $AlPO_4$ layer hydrates to form $AlPO_4 \cdot nH_2O$. This initial step may be regarded as a precursor activity because it can occur readily during storage or as a result of improper drying of the sample and can be easily reversed. Furthermore, no change of oxide morphology can be detected by the STEM. This step is characterized by a horizontal evolution in the behavior diagram.

- 27 -

Because the evolution of the surface composition during the second step of the hydration process is directly toward AlOOH, the hydration must proceed by either 1) the nucleation and growth of AlOOH without dissolution of the surface phosphate layer or 2) a slow dissolution of phosphate followed by rapid hydration of the exposed Al_2O_3. We cannot distinguish between the two possibilities with our surface composition data alone, but the following two arguments suggest that the second reaction is applicable. First, the formation of AlOOH requires the availability in solution of aluminum ions that must come from dissolution and hydrolysis of Al_2O_3, i.e., the protective phosphate layer must dissolve or become discontinuous to make the aluminum ions available. Second, and more demonstrably, Auger depth profiling indicates that less than one-fifth of the phosphate originally present (Fig. 8) is detected throughout the boehmite layer of a hydrated surface (Fig. 9). Therefore, we propose that phosphate dissolution plays an important role in the hydration of PAA surfaces. In fact, during the second step it appears to be the rate controlling process.

The third hydration step comprises the nucleation and growth of the bayerite phase, $Al(OH)_3$. The surface composition evolves along the $Al_2O_3-H_2O$ tie line, i.e., the normal hydration path of pure Al_2O_3. Although SEM micrographic and X-ray diffraction analysis indicate bayerite crystallites on top of the boehmite, the results are insufficient to determine whether the bayerite is converted from the boehmite via dissolution-redeposition or by simple nucleation in the presence of the boehmite.

- 28 -
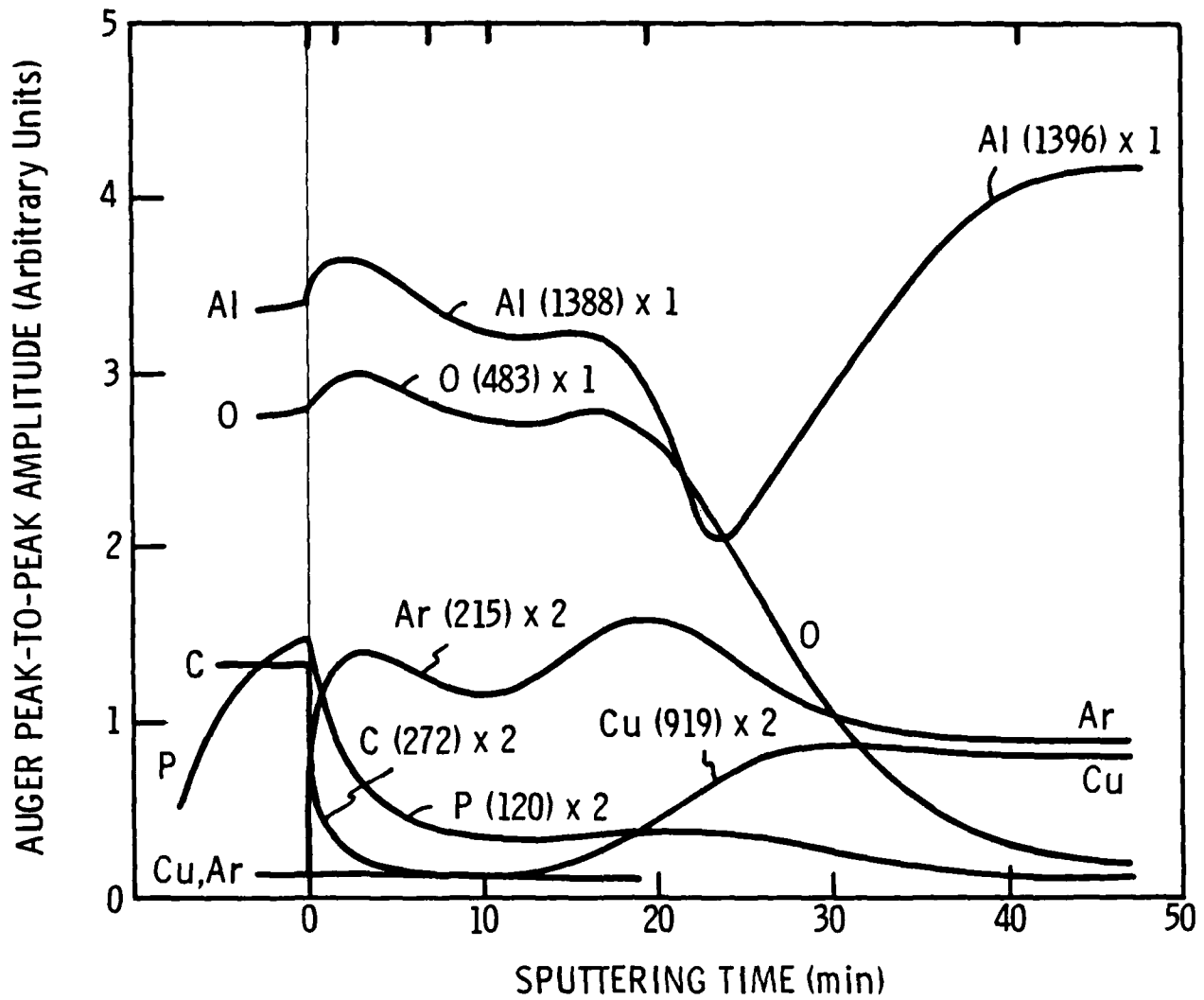
Figure 8. Auger depth profile of unhydrated PAA oxide on 2024 aluminum. The numbers in parentheses are the kinetic energies of the Auger transitions used. The relative scale for each transition is given by the number following the parentheses.
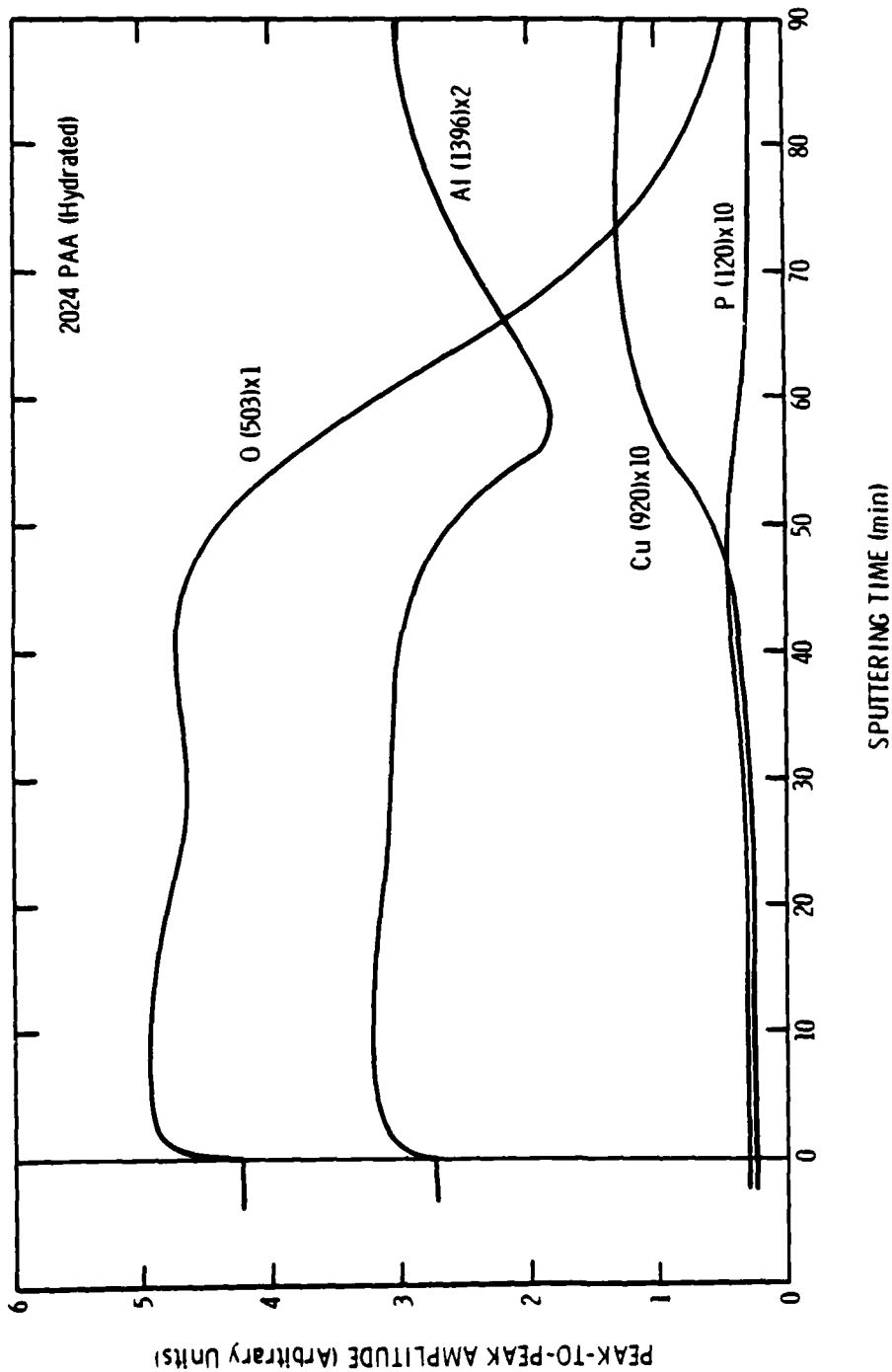
Figure 9. Auger depth profile of PAA oxide on 2024 aluminum hydrated in 100% relative humidity at 50°C for 73 hours. See the caption for Fig. 8 for explanation of the numbers beside each chemical symbol. Note that the oxygen transition is different from that used for Fig. 8. The phosphorus signal in the oxide is barely detectable above the noise level given by the copper signal in the oxide and the phosphorus signal in the metal.

All the behavior diagrams shown up to now have described the near-surface region of the samples. As mentioned earlier, the photoelectrons measured to generate the behavior diagrams have a mean free path of 4-5 atomic layers. Consequently, the signal from the outermost surface layer is only one-fourth the total signal; the behavior diagrams thus indicate the depth of the hydration products. We can adjust for this effect to derive the hydration behavior diagram for the outermost surface layer only (Fig. 10). It shows an initial monolayer of $AlPO_4$ which adsorbs water to become $AlPO_4 \cdot nH_2O$ (n < 1). Hydration continues with the nucleation of an AlOOH surface layer. Finally, the surface hydrates further to become $Al(OH)_3$.
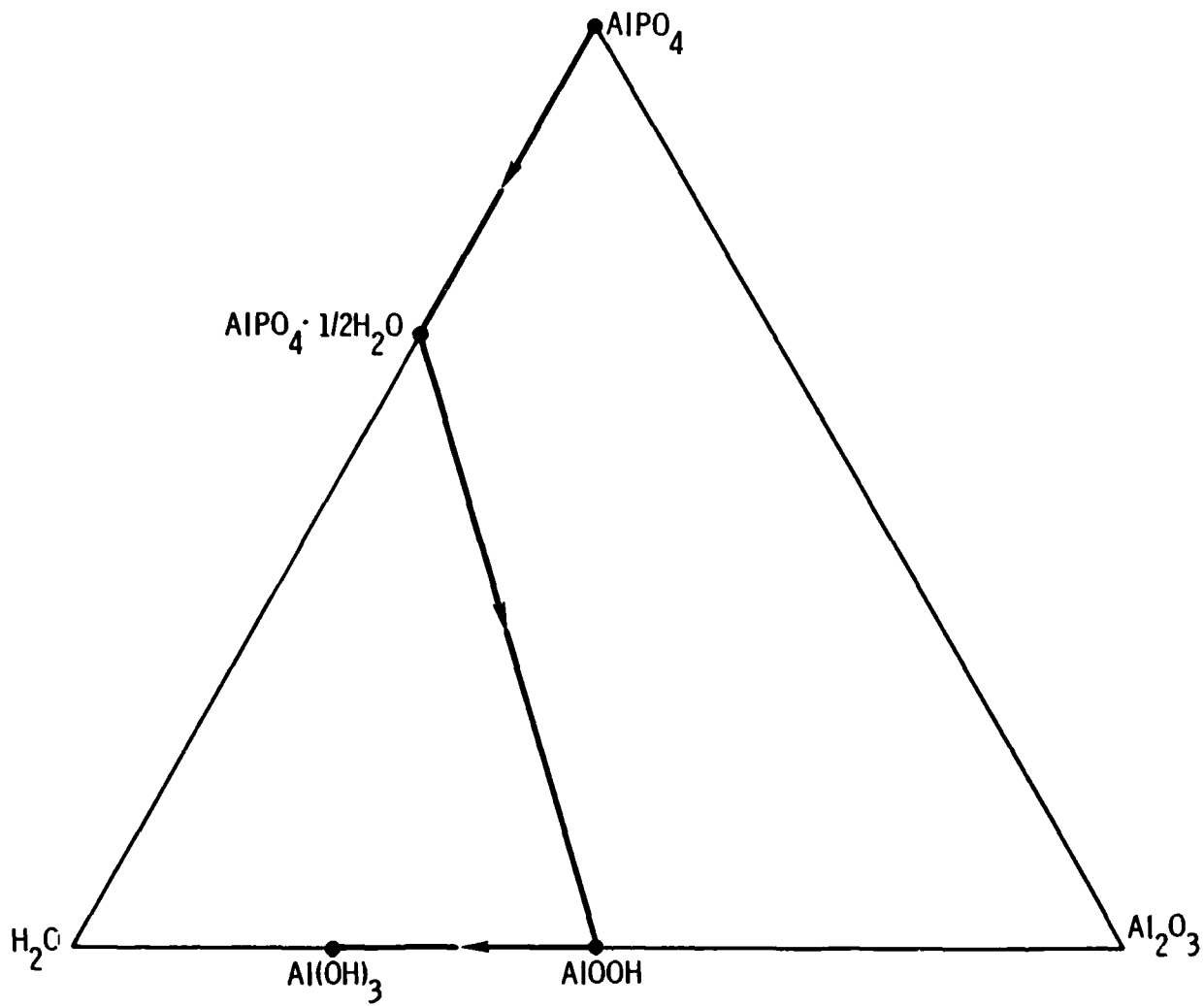
Figure 10. Surface behavior diagram of the outermost surface layer
of 2024 aluminum hydrated in 100% relative humidity at
50°C for 73 hours only. Hydration consists of three
steps: a precursor hydration of the $AlPO_4$, the nuclea-
tion and growth of $AlOOH$, and the nucleation and growth
of $Al(OH)_3$.

V. SUMMARY

By using surface behavior diagrams to trace the evolution of the
surface composition of a phosphoric-acid-anodized aluminum adherend exposed
to a water vapor-saturated atmosphere, we have shown that the hydration
process proceeds in three stages. The first stage involves the adsorption
of water by the monolayer of $AlPO_4$ present on the surface. This adsorption
occurs readily during storage, but is reversible and involves no morphological
change. In the second stage, the $AlPO_4$ monolayer slowly dissolves and
the exposed Al_2O_3 quickly hydrates to boehmite $AlOOH$. It is this
rate-limiting dissolution of the protective phosphate layer that provides
the PAA aluminum surface its superior hydration resistance and its long-
term adhesive-bond durability. In the final hydration step, the surface
hydrates further to become bayerite $Al(OH)_3$.

This three-step nature of the hydration process became evident
only upon plotting the surface composition, as a function of time, on
the $AlPO_4$-Al_2O_3-H_2O surface behavior diagram. Because changes in
the composition of surfaces as a function of time, temperature, and
other variables can be easily visualized on the appropriate surface
behavior diagrams, we expect they will become a generally useful tool to
study surface reactions.

REFERENCES

1. J.D. Venables, D.K. McNamara, J.M. Chen, T.S. Sun, and R.L. Hopping, Appl. Surf. Sci. $\underline{3}$, 88 (1979).

2. H.W. Eichner and W.E. Schowalter, Forest Products Laboratory Report No. 1813, (1950).

3. G.S. Kabayaski and D.J. Donnelly, Boeing Company Report No. D6-41517, February (1974).

4. N.W. Rogers, U.S. Patent No. 3,414,489.

5. J.D. Venables, D.K. McNamara, J.M. Chen, B.M. Ditchek, T.I. Morgenthaler, T.S. Sun, and R.L. Hopping, Proc. 12th Nat. SAMPE Symp., 909 (1980).

6. T.S. Sun, J.M. Chen, J.D. Venables, and R. Hopping, Appl. Surf. Sci. $\underline{1}$, 202 (1978).

7. P.W. Palmberg, J. Vac. Sci. Technol. $\underline{12}$, 379 (1975).

8. D. Menetrier, I. Jawed, T.S. Sun, and J. Skalny, Cem. Concr. Res. $\underline{9}$, 473 (1975).

9. C.D. Wagner, W.M. Riggs, L.E. Davis, J.F. Moulder, and G.E. Muilenberg, Handbook of X-ray Photoelectron Spectroscopy, (Perkin-Elmer Corporation, Physical Electronics Division, Eden Praire, MN, 1979).

10. T.S. Sun, D.K. McNamara, J.S. Ahearn, J.M. Chen, B.M. Ditchek, and J.D. Venables, Appl. Surf. Sci. $\underline{5}$, 406 (1980).

11. J.S. Ahearn, T.S. Sun, C. Froede, J.D. Venables, and R.L. Hopping, SAMPE Q. $\underline{12}$, 39 (1980).

12. W. Vedder and D.A. Vermilyea, Trans. Faraday Soc. $\underline{65}$, 561 (1969).

13. J.P. O'Sullivan, J.A. Hockey and G.C. Wood, Trans. Faraday Soc. $\underline{65}$, 535 (1969).

14. D.R. Penn, J. Electron Spectrosc. Relat. Phenom. $\underline{9}$, 29 (1976).

15. D.A. Vermilyea and W. Vedder, Trans. Faraday Soc. $\underline{66}$, 2649 (1970).

16. J.S. Ahearn, G.D. Davis, and J.D. Venables (to be published).